

DT#43635 QA:NA CB7/27/86

THE ELECTROCHEMICAL BEHAVIOR OF ALLOY 22 IN EXTREME CHLORIDE AND NITRATE ENVIRONMENTS

R.A. Etien*, S.R. Gordon and G.O. Ilevbare⁺
Lawrence Livermore National Laboratory
Livermore, CA 94550

ABSTRACT

Alloy 22 specimens were tested in high temperature (100 to 160°C), high concentration chloride and nitrate environments. Results of this study indicate that increasing nitrate to chloride ratio to 0.5 in these electrolytes increases resistance to localized breakdown and enhances repassivation. In these extreme environments, localized corrosion occurred by pitting even though specimens were tested using artificial crevice formers. Open circuit (E_{corr}), breakdown and repassivation potentials all increase, and pitting morphology changes as nitrate to chloride ratio increases from 0.05 and 0.15 to 0.5. Results also indicate that increasing the temperature from 100 to 160°C increases E_{corr} values, while breakdown potentials and repassivation potentials peak at 130°C for the 0.5 nitrate to chloride ratio electrolytes.

Keywords: Alloy 22, localized corrosion, nitrate, chloride, welds, deliquescence

INTRODUCTION

Alloy 22 is a nickel-based alloy that is highly corrosion resistant. It falls into the general category of nickel-chromium-molybdenum alloys known for their high corrosion resistance. Like other alloys in this family, Alloy 22 exhibits both low general corrosion rates and high resistance to localized corrosion in a wide range of environments.¹⁻⁸

Alloy 22 is the corrosion barrier material for the waste packages intended for the underground disposal of radioactive waste at Yucca Mountain. One of the most probable exposure mechanisms of the waste packages to aqueous solutions will be through the process of deliquescence. Deliquescence is the process by which a crystalline solid absorbs moisture and subsequently dissolves. As the waste packages cool and the relative humidity rises, the likelihood of deliquescence occurring on the package surface increases. The initial solutions that form through this process are predicted to exist at high temperatures (probably above 100°C) and contain high salt concentrations.^{9, 10}

Solutions containing high amounts of chloride and nitrate have been identified as one type of deliquescence solution that can form in the repository.¹⁰ Nitrate has been shown to have an inhibitive

* Knolls Atomic Power Laboratory, Schenectady, NY

⁺ Integrated Science Solutions Inc., Walnut Creek, CA

effect on the localized corrosion behavior of Alloy 22 in chloride solutions at lower concentrations and temperatures than those used in this study.^{2, 3, 7, 11} Dunn and Brossia found that for welded Alloy 22 specimens tested in 0.5 M NaCl solutions at 95°C, there was no crevice corrosion initiated in potentiodynamic tests for nitrate to chloride ratios of 0.2 or greater but crevice corrosion did occur at ratios of 0.1 and below.³ Evans et. al. found that in potentiodynamic testing of Alloy 22 in 5 M calcium chloride (CaCl₂) solutions, the onset of localized corrosion could be shifted from 75°C to 105°C by adding 0.5 M calcium nitrate (Ca(NO₃)₂).² As the ratio of nitrate to chloride is increased, an increase in both breakdown potentials and repassivation potentials occurs, and the difference between these potentials and open circuit values increases.^{2, 3, 7, 11} In this study the effect of nitrate on localized corrosion of welded Alloy 22 specimens at extremes of chloride concentration and temperature in CaCl₂ + Ca(NO₃)₂ solutions was examined.

EXPERIMENTAL

Alloy 22 specimens were prepared from welded plate specimens. The welds were made by means of Gas Tungsten Arc Welding (GTAW). These specimens (Figure 1) were set up in a multiple crevice assembly (MCA) based on crevice formers described by the American Society for Testing and Materials (ASTM) in ASTM G 48.¹² In addition to the Alloy 22 specimen, the MCA set-ups consisted of ceramic crevice formers and titanium grade 2 bolts, nuts and washers. A layer of polytetrafluoroethylene (PTFE) tape was inserted between the crevice formers and the specimens in order to fill any microvoids and create reproducibly tight crevices. The surface of the titanium bolt was insulated from the specimen using polyolefin shrink fit tubing. Crevice formers were tightened to a torque of 70 in-lbs.

The working surfaces on the MCA specimens were polished to a 600-grit finish using SiC paper. The areas perpendicular to the surface on which the crevice former rested (edge of specimen) were sequentially polished using 100, 240 and 600 grit papers in order to remove any damage done by electric discharge machining (EDM) during fabrication of the specimens by the supplier. After polishing, the specimens were sequentially degreased using hexane, acetone and methanol. After degreasing the specimens were assembled.

Electrochemical testing was conducted using a three-electrode setup with a saturated silver/silver chloride (SSC) reference electrode and a platinum counter electrode measuring roughly 40 cm² in surface area. The reference electrode was cooled using a cooling jacket with flowing water maintained at 5 to 12°C, in order to keep the reference electrode temperature near 25°C. A water-cooled condenser was also used to minimize evaporative concentrating of solutions. Solutions were deaerated using nitrogen gas flowing at a rate of 50 to 100 cc per minute. Nitrogen escaping from the condenser outlet was bubbled through a water trap in order to avoid any backflow of oxygen from the air.

For each specimen tested, three different electrochemical tests were conducted in succession without renewing the specimen surface. First, open circuit potential (E_{corr}) was monitored for twenty-four (24) hours followed by a series of polarization resistance tests from which passive corrosion rates were calculated (these will not be discussed). Finally a cyclic potentiodynamic polarization (CP) test was performed. The CP scans started at approximately 100 mV below the 24hr corrosion potential (E_{corr}) and continued until a current density of 5 mAcm⁻² or a maximum voltage reading of up to 1 V (SSC) was reached before the scan was reversed. The scan rate used for the forward and reverse sweeps was 0.1667 mVs⁻¹.

Nine different solutions under eleven different conditions were used for testing. These are tabulated

in Table 1. Three different CaCl_2 compositions were chosen. For each CaCl_2 composition, $\text{Ca}(\text{NO}_3)_2$ was added in order to generate a nitrate to chloride ratio ($\text{NO}_3^-:\text{Cl}^-$ ratio) of 0.05, 0.15, or 0.5. It was necessary to use three different CaCl_2 concentrations, in order to cover the desired temperature range of 100 to 160°C. The 160°C solutions are solid at 100°C, and the 100 and 130°C solutions boil at 160°C. The 12 molal CaCl_2 + 6 molal $\text{Ca}(\text{NO}_3)_2$ solution was used at three different test temperatures to investigate the effect of temperature on the measured parameters. Calcium chloride dihydrate and calcium nitrate tetrahydrate used to prepare the electrolytes met reagent grade purity requirements set by the American Chemical Society (ACS).

Cyclic polarization data was analyzed for breakdown potential (E_{20}) and for repassivation potential (E_{r1}). E_{20} is the potential where current density first reaches $20 \mu\text{Acm}^{-2}$ on the forward anodic scan of the polarization curve. It is a measure of resistance to initiation of localized corrosion. E_{r1} is the potential where a decaying current density reaches $1 \mu\text{Acm}^{-2}$ on the reverse scan of the polarization curve, that is, below the chosen potential, the current density consistently remains below a current density of $1 \mu\text{Acm}^{-2}$ in the anodic portion of the reverse scan. The repassivation potential E_{r1} is a measure of how easily a specimen repassivates once localized corrosion has initiated, and represents the potential below which self sustaining localized corrosion is not expected to occur.

RESULTS

Figure 2 shows 24 hour E_{corr} values plotted against temperature (bottom x-axis) and CaCl_2 concentration (top x-axis) for the different $\text{NO}_3^-:\text{Cl}^-$ ratios. The lines shown in the plots are interpolation lines used as aids to show trends in the data. They have no other physical meaning. It can be seen that the 0.5 $\text{NO}_3^-:\text{Cl}^-$ ratio solutions show more noble E_{corr} values compared with 0.05 and 0.15 ratio solutions at constant temperature and chloride concentration ($[\text{Cl}^-]$) in the 130 and 160°C electrolytes (moving vertically). For the 100°C electrolytes, this trend is not apparent due to large scatter in the E_{corr} values for the 0.15 $\text{NO}_3^-:\text{Cl}^-$ ratio electrolyte. The E_{corr} values also show a tendency to increase with electrolyte concentration ($[\text{Cl}^-]$ and $[\text{NO}_3^-]$) and temperature. Increasing temperatures correspond to increasing Cl^- and NO_3^- (solute) concentrations. Note that the CaCl_2 concentrations shown in Figure 2 (and subsequent figures) are not plotted to scale, but are used to delineate the data points with their corresponding CaCl_2 concentrations.

Figures 3 and 4 show examples of polarization curves taken in these extreme environments. Figure 3 is a polarization curve for a specimen tested in 10 molal CaCl_2 + 5 molal $\text{Ca}(\text{NO}_3)_2$ at 100°C. The curve exhibits a large intermediate peak on the forward scan that reaches a maximum near 0.4 V. E_{20} is reached at 0.208 V on the forward scan. A further increase in potential results in the stepwise drop of the current density of the specimen until repassivation occurs at about 750 mV. A further increase in the potential results in another increase in current, this time due to either transpassive dissolution or oxygen evolution. This was confirmed by visual inspection of the specimen, and by the fact that a reversal of the potential at 1 V does not result in a hysteresis loop, which would have been indicative of localized breakdown. This is similar to the behavior observed for Alloy 22 in 5 M CaCl_2 at between 60 and 75 °C.¹³ The curve also shows some unconventional behavior on its reverse scan. The current density immediately begins to drop when the current scan is reversed at 1 V. The current density drops below $1 \mu\text{Acm}^{-2}$ at 0.691 V. This trend continues until the reverse scan changes to cathodic behavior for a very small potential range (0.525 to 0.490 V), implying the reduction of an oxidized specie (probably oxidized during the forward scan). At roughly 0.490 V, the current density once again switches back to anodic behavior and the current density increases to values above $1 \mu\text{Acm}^{-2}$ and reaches a peak of $60 \mu\text{Acm}^{-2}$ near 0.25 V before decreasing below $1 \mu\text{Acm}^{-2}$ once again at 0.078 V, this

time permanently. For a polarization curve showing reactivation behavior like this, the E_{r1} value is the second potential value (lowest value) where current density drops below $1 \mu\text{Acm}^{-2}$, in this case 0.078 V.

Figure 4 shows three polarization curves taken for the three different $\text{NO}_3^-:\text{Cl}^-$ ratios for 12 molal CaCl_2 at 130°C . The polarization curves for the 0.05 and 0.15 $\text{NO}_3^-:\text{Cl}^-$ ratio solutions both exhibit passive behavior spanning 200 mV or less and show significant hysteresis behavior on the reverse scan. They both reach their reverse current density criterion of 5mAcm^{-2} before reaching the reverse potential criteria of 1 V. The scan for the 0.5 $\text{NO}_3^-:\text{Cl}^-$ ratio solution, however, exhibits a larger passive range and shows a relatively smaller hysteresis loop. It does not reach the reverse current density before reaching 1 V. This series of curves exhibits a trend of increasing breakdown and repassivation potentials with increasing $\text{NO}_3^-:\text{Cl}^-$ ratio.

Figure 5 shows E_{20} versus temperature at various CaCl_2 concentration. E_{20} increases as the $\text{NO}_3^-:\text{Cl}^-$ ratio increases at a given temperature and $[\text{Cl}^-]$. The data shows there is a large increase in E_{20} at the higher temperatures (130 and 160°C) and highest 0.5 $\text{NO}_3^-:\text{Cl}^-$ ratio compared with the lower 0.05 and 0.15 ratios. In the lowest temperature, lowest concentration electrolytes (100°C and 10 molal CaCl_2), there is still a positive effect on the breakdown potentials (increase) from increasing $\text{NO}_3^-:\text{Cl}^-$ ratios, but it is not as dramatic as the increase in the 130 and 160°C electrolytes. E_{20} values also generally show an increase when moving to higher temperatures and concentrations ($[\text{Cl}^-]$ and $[\text{NO}_3^-]$) for constant $\text{NO}_3^-:\text{Cl}^-$ ratio except when moving from 130 to 160°C for 0.5 $\text{NO}_3^-:\text{Cl}^-$ ratio electrolytes. The increase is especially dramatic when moving from 100 to 130°C in the 0.5 $\text{NO}_3^-:\text{Cl}^-$ ratio electrolytes.

Figure 6 shows E_{r1} versus temperature at various CaCl_2 concentrations. The data shows similar trends to E_{20} data (Figure 5). Higher $\text{NO}_3^-:\text{Cl}^-$ ratios, at a constant temperature and $[\text{Cl}^-]$, result in higher E_{r1} values for Alloy 22. For a given $\text{NO}_3^-:\text{Cl}^-$ ratio, E_{r1} increases as $[\text{Cl}^-]$ and $[\text{NO}_3^-]$ increase. More dramatic increases in E_{r1} take place in the presence of solutions with a 0.5 $\text{NO}_3^-:\text{Cl}^-$ ratio, and is consistent with observations made in Figure 5 for E_{20} values.

In general, the trends seen with both E_{20} and E_{r1} are similar to those seen for E_{corr} values. They all show the tendency to move toward more noble values as $\text{NO}_3^-:\text{Cl}^-$ ratio is increased and also as solutions at a constant $\text{NO}_3^-:\text{Cl}^-$ ratio become more concentrated and are tested at higher temperatures. The effect of $[\text{Cl}^-]$ (or absolute concentration) and temperature does not appear to be as strong as the effect of $\text{NO}_3^-:\text{Cl}^-$ ratio or absolute $[\text{NO}_3^-]$ (Figures 2, 5 and 6).

To help determine the separate effects of temperature and solute concentration on the E_{20} , E_{r1} and E_{corr} of Alloy 22 in these extremely concentrated electrolytes; another series of experiments was conducted. For these experiments a constant electrolyte concentration of 12 molal CaCl_2 + 6 molal $\text{Ca}(\text{NO}_3)_2$ was used while the testing temperature was varied between 100 and 150°C . Figure 7 compares the cyclic polarization behavior of specimens tested in the 12 molal CaCl_2 + 6 molal $\text{Ca}(\text{NO}_3)_2$ electrolytes at 100 , 130 and 150°C . The curves at 100 and 130°C exhibit intermediate peaks on the forward scan not present in the 150°C curve. The presence of two anodic/cathodic transitions during the reverse scan of the 100°C curve mentioned previously (Figure 3) can also be seen in Figure 7. Figure 8 shows 24-hour E_{corr} , E_{20} and E_{r1} of Alloy 22 as a function of temperature in 12 molal CaCl_2 + 6 molal $\text{Ca}(\text{NO}_3)_2$. 24-hour E_{corr} values show a consistent increase as a function of temperature. Both the E_{20} and E_{r1} values of Alloy 22 in this electrolyte show an increase between 100 and 130°C and then a decrease in values between 130 and 150°C . Thus, maximum resistance to localized corrosion in this electrolyte is shown at 130°C for Alloy 22. This is a parabolic relationship rather than a linear one.

Observations of all specimens tested in this study showed that localized corrosion occurred on all but one specimen. This specimen was tested in 0.5 $\text{NO}_3^-:\text{Cl}^-$ ratio solution at 160°C. The localized corrosion mechanism for all specimens was pitting. Crevice corrosion was not observed, in spite of the fact that specimens were multiple crevice assemblies (MCA). Figure 9 shows an example of the pitting seen on a specimen tested in 12 molal CaCl_2 + 0.6 molal $\text{Ca}(\text{NO}_3)_2$ at 130°C. Most of the pitting on this specimen is on the outer portion of the specimen and takes on a light gray appearance in the image. Pitting showed no evidence of preferential initiation at crevice formers on this or any other samples. Total pitted area became smaller and pit aspect ratio (width to depth) became larger (pitting became shallower) as $\text{NO}_3^-:\text{Cl}^-$ ratio increased. The total pitted area on all specimens tested in 0.5 $\text{NO}_3^-:\text{Cl}^-$ ratio electrolytes was small relative to other specimens. Among the 0.5 $\text{NO}_3^-:\text{Cl}^-$ ratio specimens, those tested at 100°C showed the most pitting.

Pitted zones took on a different appearance in weld versus base zones of the specimen. Figure 10 shows a dark field light microscopy image of pitting at a weld/base metal interface. Most of the surface shown in this image is pitted with pitted areas showing up as light gray or gray in color. In the weld zone, pitting preferentially occurred on the dendrites. The dendrites tend to be depleted in Mo, and the interdendrites are usually enriched in Mo). . In the base metal zone, pitting occurred randomly, without a preferred area of attack. Pitting did not appear to show a preference toward attack of weld or base metal for these cyclically polarized specimens. Dark field is used in Figure 10 to show the features inside the pitted areas, because pits show up as featureless dark areas in bright field images.

DISCUSSION

Results of the current study indicate that in high temperature, high concentration CaCl_2 + $\text{Ca}(\text{NO}_3)_2$ bearing electrolytes the $\text{NO}_3^-:\text{Cl}^-$ ratio has a strong influence on E_{corr} , breakdown potentials, E_{20} , and repassivation potentials, E_{r1} . These results are consistent with those of other researchers who studied the behavior of Alloy 22 at, lower temperatures, in lower chloride concentration bearing environments.^{2,3,7, 11} These results therefore imply that the inhibiting ability of nitrate on localized corrosion is maintained at extremes of chloride concentration and temperature provided that critical ratios of $\text{NO}_3^-:\text{Cl}^-$ are maintained.

24 hour E_{corr} values are higher for 0.5 $\text{NO}_3^-:\text{Cl}^-$ ratio solutions than for 0.05 or 0.15 $\text{NO}_3^-:\text{Cl}^-$ ratio solutions tested at 130 and 160°C (Figure 2). Figure 8 shows that the major contributor to the increase in corrosion potential seen in Figure 2 is temperature. The E_{corr} values shown in Figure 8 roughly correspond to the values for the 0.5 $\text{NO}_3^-:\text{Cl}^-$ ratio curve from Figure 2. This implies that kinetic effects are important in determining the corrosion potential of Alloy 22 in these electrolytes. Reaction kinetics generally increase with temperature. Nonetheless, E_{corr} , as well as E_{20} data indicates that in these electrolytes, nitrate helps to maintain a more effective passivation layer on the Alloy 22 surface in these environments.

Breakdown potentials also increase significantly as the $\text{NO}_3^-:\text{Cl}^-$ ratios increase from 0.05 to 0.5 at test temperatures of 130 and 160°C (Figure 5). This increase is even larger in magnitude than it is for the E_{corr} values and is consistent with the increase in the passive region of Alloy 22 as observed in Figure 4. These results suggest that the higher corrosion potentials registered on Alloy 22 in the 0.5 $\text{NO}_3^-:\text{Cl}^-$ ratio electrolytes translate to more resistant oxide films, and thus higher breakdown and repassivation potentials (Figures 2, 5 and 6). Breakdown and repassivation potentials indicate that nitrate effectively raises breakdown and repassivation to higher potentials, and implies that localized corrosion is more difficult to initiate and repassivation is enhanced as nitrate concentration increases in

solution. This is particularly evident at higher temperatures and higher $[Cl^-]$. E_{20} and E_{r1} values are much higher for the 0.5 $NO_3^-:Cl^-$ ratio electrolytes under the 130 and 160°C testing condition shown in Figures 5 and 6. In fact the very small pitted areas (a few square mm or less) and the small hysteresis loop for the 0.5 $NO_3^-:Cl^-$ ratio specimens tested at 130°C and above suggest that transpassive dissolution or oxygen evolution currents were the dominant processes at high potentials and partially explains the high E_{20} values for these electrolytes (Figures 5 and 8).

The relationship between E_{20} and temperature is unusual (Figure 8). The increase of E_{20} as temperature is increased suggests that temperature increases the breakdown potential of Alloy 22 instead of reducing it as is usually observed in experiments of this nature. The same argument can be made for E_{r1} values, however, there is some scatter in the 130°C and 150°C E_{r1} values that makes this conclusion less substantiated. A couple of possibilities exist as to why E_{20} first increased with temperature before decreasing upon further increase in temperature. It is possible that increases in temperature allowed thicker, more resistant oxide film to form at temperatures within the test duration time due to higher kinetic energy (ionic mobility) in the system at these high temperatures. This film could counteract the higher dissolution rates that are often associated with higher temperature electrolytes. The ability to grow thicker (rather than thinner) oxide films with increase in temperature might be explained by increase in activity of ions in the electrolyte with increase in temperature. The consistency of the electrolyte used is viscous at 100°C. It solidifies between 80 and 90°C. So it is not unreasonable to expect that the activity of the ions in the electrolyte will increase as temperature is increased. However, after a certain temperature, any improvement due to increased activity diminishes, and further temperature increases result in a reduction of E_{20} . Thus, while further increases in temperature above 130°C (in this case) may not lead to thinner or less robust oxide films (as E_{corr} increases with temperature, Figure 8), the increased mobility of Cl^- ions in solution and their ability to cause reductions in E_{20} start to exceed the ability of any improvement in the oxide film to mitigate localized breakdown. However, the effect of temperature on the breakdown potentials of Alloy 22 may be due to more than just a simple case of thickening the oxide film at the higher temperatures. The presence of the large anodic peak at 100°C in Figure 3 could result from a change in the composition and/or structure of the passive film (also applies to Figure 7). Such changes may also be facilitated by a change in the activity of the ions in solution. It is possible that one component of the film is being dissolved and replaced by another. The fact that this peak occurs at a potential that is higher than what is seen for a simple active to passive transition lends support to this possibility. This peak is still present on the 130°C curve, but it is not as prominent. The 150°C curve does not display any peak, which suggests that the passive film is not going through the significant changes that are potentially occurring at the lower temperatures or proceeds through this transition at a rate faster than can be registered on the polarization curves. It can be observed that the passive current density of Alloy 22 increases with increase in temperature (Figure 7).

CONCLUSIONS

- The ability of nitrate to inhibit localized corrosion of welded Alloy 22 specimens is maintained in high concentration, high temperature $CaCl_2 + Ca(NO_3)_2$ electrolytes.
- Welded Alloy 22 specimens tested in $NO_3^-:Cl^-$ ratios of 0.5 show higher resistance to localized corrosion than specimens tested at ratios of 0.15 and 0.05. Breakdown and repassivation values as well as E_{corr} increase when $NO_3^-:Cl^-$ ratio is increased to 0.5 from 0.05 or 0.15.
- Increasing the $NO_3^-:Cl^-$ ratio to 0.5 from 0.05 or 0.15 in these electrolytes widens the range of passive behavior.
- In 0.5 $NO_3^-:Cl^-$ ratio solutions with constant electrolyte concentrations, E_{corr} values increase with

increasing temperature, while E_{20} and E_{r1} values peak at 130°C.

- Pit morphology changes as nitrate to chloride ratio increases. At low ratios pits tend to be deeper than at high ratios.

ACKNOWLEDGEMENTS

This work was performed under the auspices of the U.S. Department of Energy by the University of California Lawrence Livermore National Laboratory under contract No. W-7405-Eng-48. This work is supported by the Yucca Mountain Project, which is part of the Office of Civilian Radioactive Waste Management (OCRWM).

REFERENCES

1. J. C. Farmer, R. D. McCright, G. E. Gdowski, F. Wang, T. S. E. Summers, P. Bedrossian, J. M. Horn, T. Lian, J. C. Estill, A. Lingenfelter and W. Haalsey, PVP-ASME, 408, 53 (ASME 2000: New York, NY).
2. K. J. Evans, S. D. Day, G. O. Ilevbare, M. T. Whalen, K. J. King, G. A. Hurst, L. L. Wong, J. C. Estill and R. B. Rebak, *Transportation, Storage, and Disposal of Radioactive Materials*, PVP-Vol. 467, p. 55 (2003).
3. D. S. Dunn and C. S. Brossia, paper 02548, CORROSION 2002, NACE International, Houston, TX (2002).
4. N. S. Meck, P. Crook, S. D. Day and R. B. Rebak, Paper 03, CORROSION 2003, NACE International, Houston, TX (2003).
5. L. L. Wong, D. V. Fix, J. C. Estill, R. D. McCright and R. B. Rebak, 26th Symposium on the Scientific Basis for Nuclear Waste Management as held at the 2002 MRS Fall Meeting; Boston, MA, USA, 2-5 Dec. 2002. pp. 735-742. 2003.
6. R. B. Rebak and P. Crook, Paper 00499, CORROSION 2000, NACE International, Houston, TX (2000).
7. B. A. Kehler, G. O. Ilevbare and J. R. Scully, *Corrosion*, 57, pp. 1042-1065; 2001.
8. R. B. Rebak and J. C. Estill, 26th Symposium on the Scientific Basis for Nuclear Waste Management as held at the 2002 MRS Fall Meeting, Boston, MA, USA, 2-5 Dec. 2002. pp. 713-722. 2003.
9. G. E. Gdowski. "W1045 Environment on the Surfaces of the Drip Shield & Waste Package Outer Barrier", LLNL, Report ANL-EBS-MD-000001.
10. J. Farmer, V. Pasupathi, P. Nair, G. Gordon, D. McCright, G. Gdowski, S. Carroll, T. Steinborn, T. Summers, F. Wong, R. Rebak, R. Lian, G. Ilevbare, J. Lee, F. Hua and J. Payer, "Technical Basis Document No. 6: Waste Package and Drip Shield Corrosion", UCRL-LR-155288.
11. G. O. Ilevbare, K.J. King, S.R. Gordon, H.A. Elayat, G.E. Gdowski, and T.S.E. Gdowski, Effect of Nitrate on the Repassivation Potential of Alloy 22 in Chloride Containing Environments. To be published in the Journal of the Electrochemical Society.
12. American Society for Testing and Materials, Annual Book of ASTM Standards, Vol.03.02, West Conshohocken, PA: ASTM (2001).
13. G.O. Ilevbare, Electrochemical Behavior of Alloy 22 in 5 M CaCl₂, in Transportation Storage, and Disposal of Radioactive Materials-2002, Edited by R.S. Hafner, p.55, PVP-Vol. 449, 2002. Paper Number PVP2002-1614, American Society of Mechanical Engineers, 2002 Pressure Vessels and Piping Conference, August 4-8, 2002, Vancouver, British Columbia, Canada.

TABLE 1 - THE TEST ELECTROLYTES

CaCl ₂ Concentration	Ca(NO ₃) ₂ Concentrations	Temperature
10 molal	0.5 molal, 1.5 molal, 5 molal	100°C
12 molal	0.6 molal, 1.8 molal, 6 molal	130°C
12 molal	6 molal	100, 150°C
18 molal	0.9 molal, 2.7 molal, 9 molal	160°C

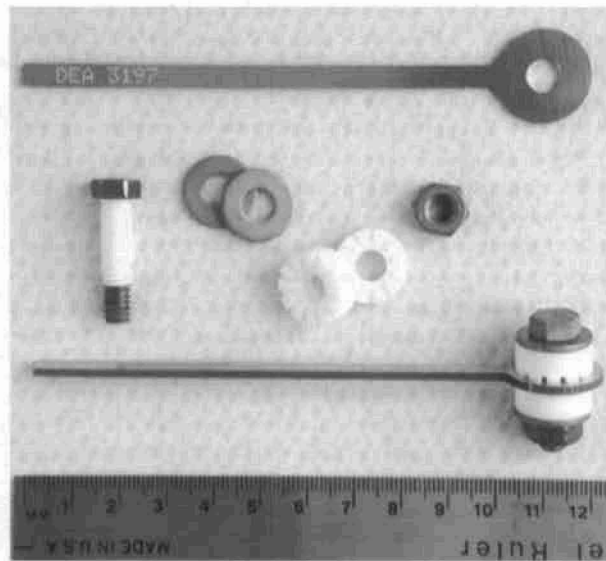


FIGURE 1 - Multiple crevice assembly (MCA) showing lollipop specimens with ceramic crevice formers and titanium grade 2 bolt, nut and washers.

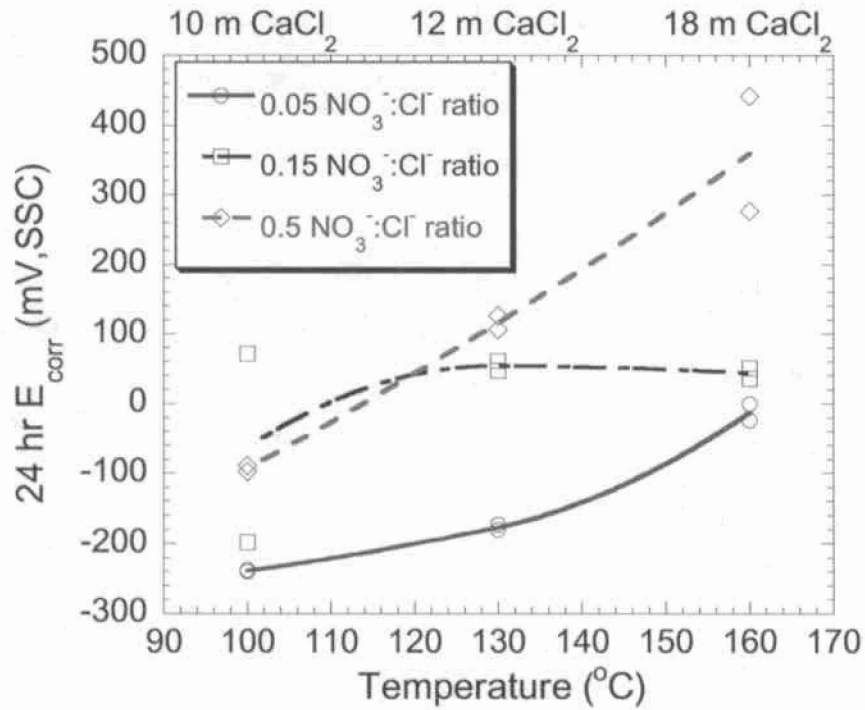


FIGURE 2 - 24 hour E_{corr} values versus temperature (bottom x-axis) and $CaCl_2$ concentration (top x-axis) for 0.05, 0.15 and 0.5 $NO_3^-:Cl^-$ ratios.

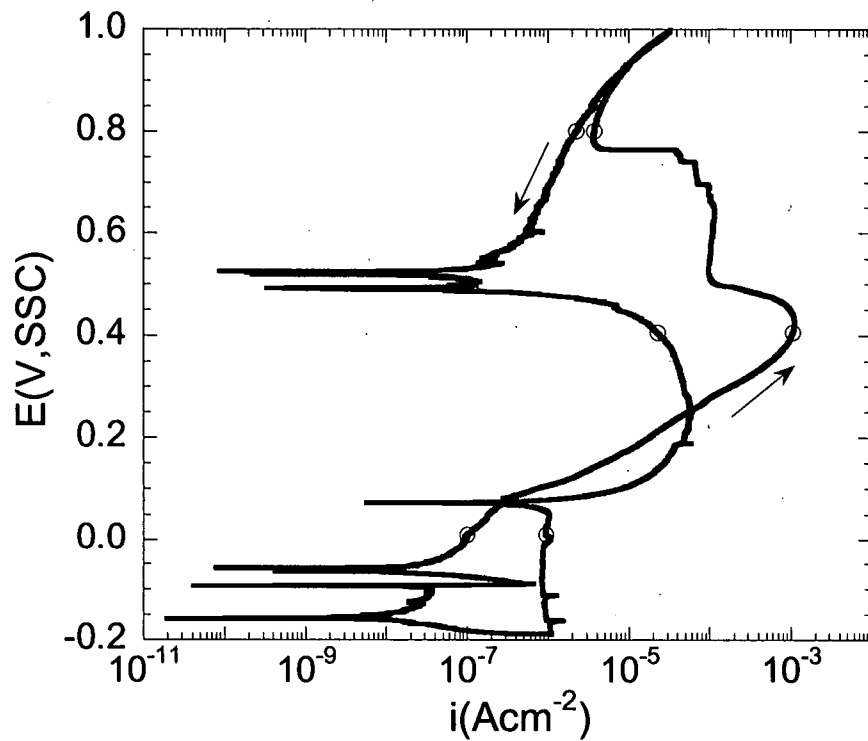


FIGURE 3 - Cyclic polarization curve for specimen tested in 10 molal CaCl_2 + 5 molal $\text{Ca}(\text{NO}_3)_2$ at 100°C .

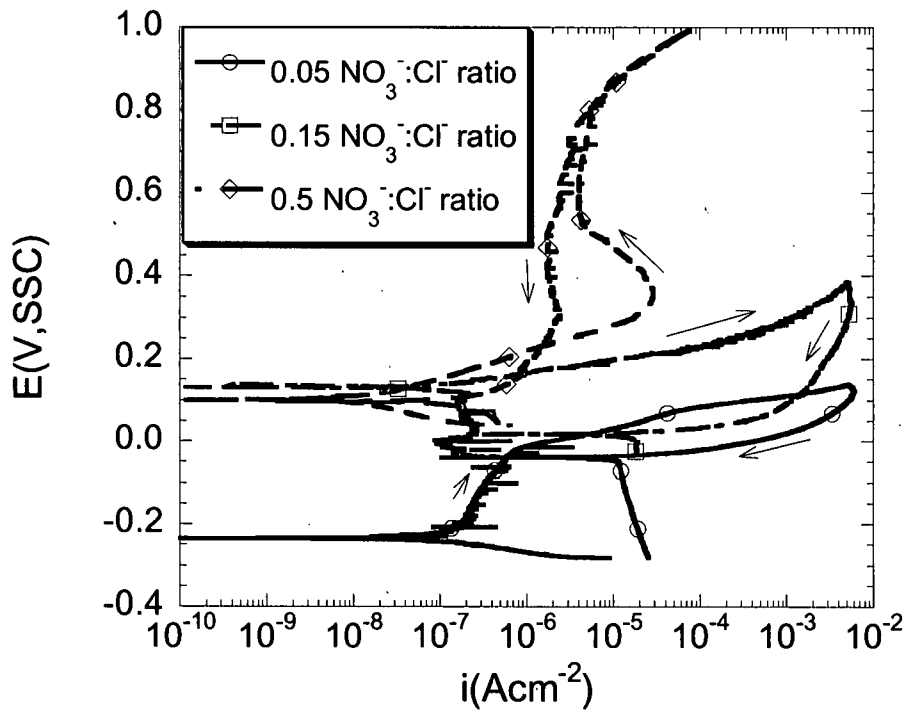


FIGURE 4 - Comparison of polarization curves for 0.05, 0.15 and 0.5 $\text{NO}_3^-:\text{Cl}^-$ ratios containing 12 molal CaCl_2 at 130°C .

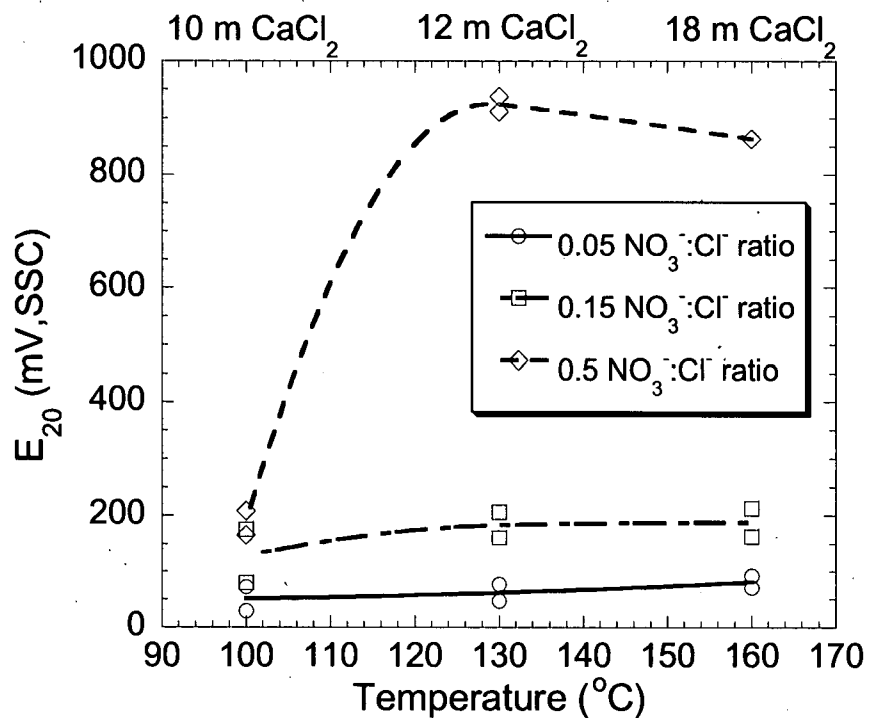


FIGURE 5 - E_{20} values versus temperature (bottom x-axis) and CaCl_2 concentration (top x-axis) for 0.05, 0.15 and 0.5 $\text{NO}_3^-:\text{Cl}^-$ ratios.

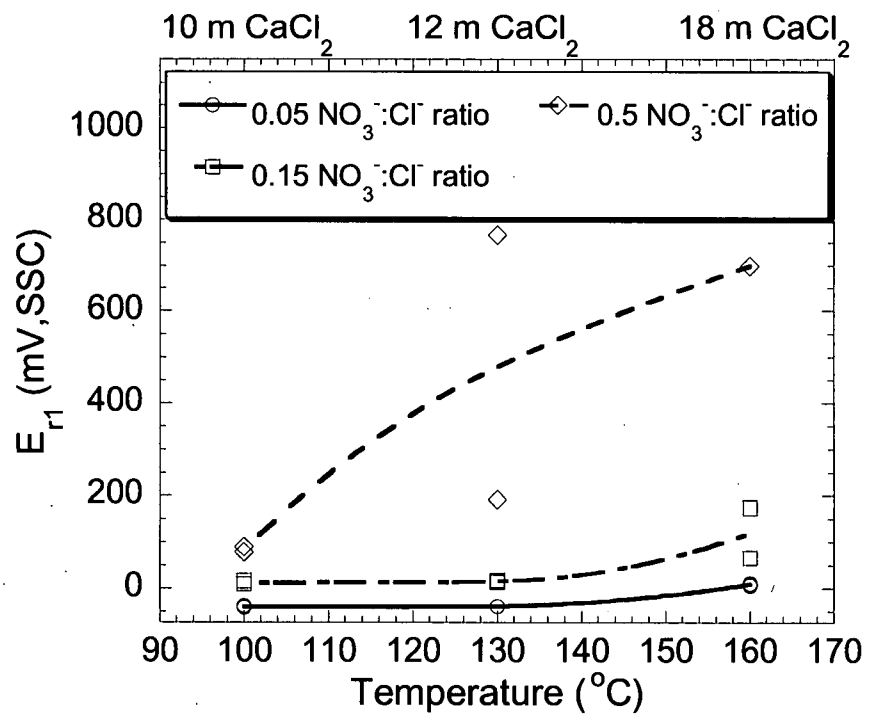


FIGURE 6 - E_{r1} values versus temperature (bottom x-axis) and CaCl_2 concentration (top x-axis) for 0.05, 0.15 and 0.5 $\text{NO}_3^-:\text{Cl}^-$ ratios.

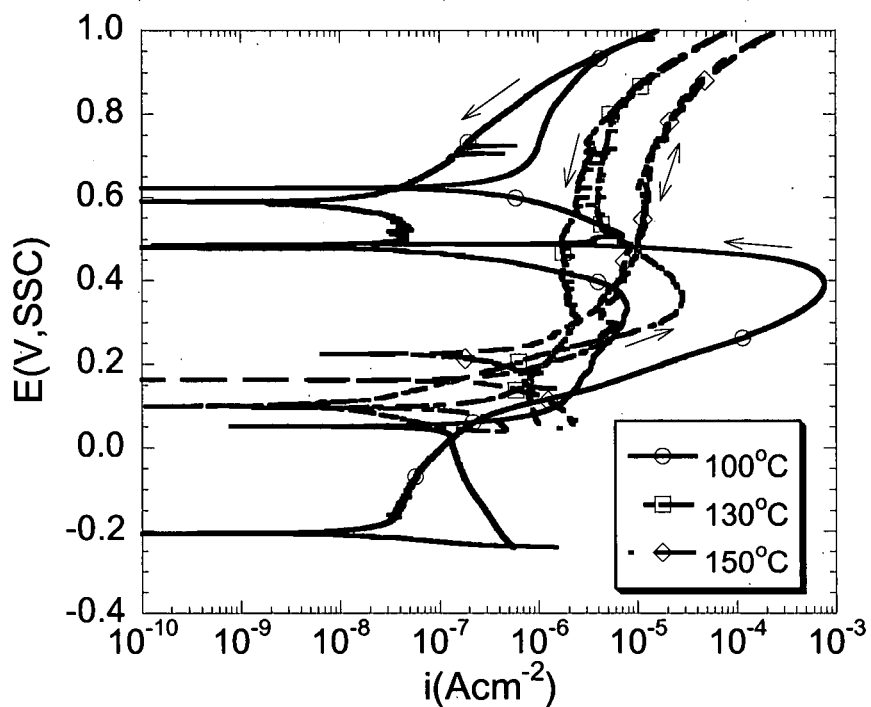


FIGURE 7 - Comparison of polarization curves for 12 molal CaCl_2 + 6 molal $\text{Ca}(\text{NO}_3)_2$ at 100, 130 and 150°C.

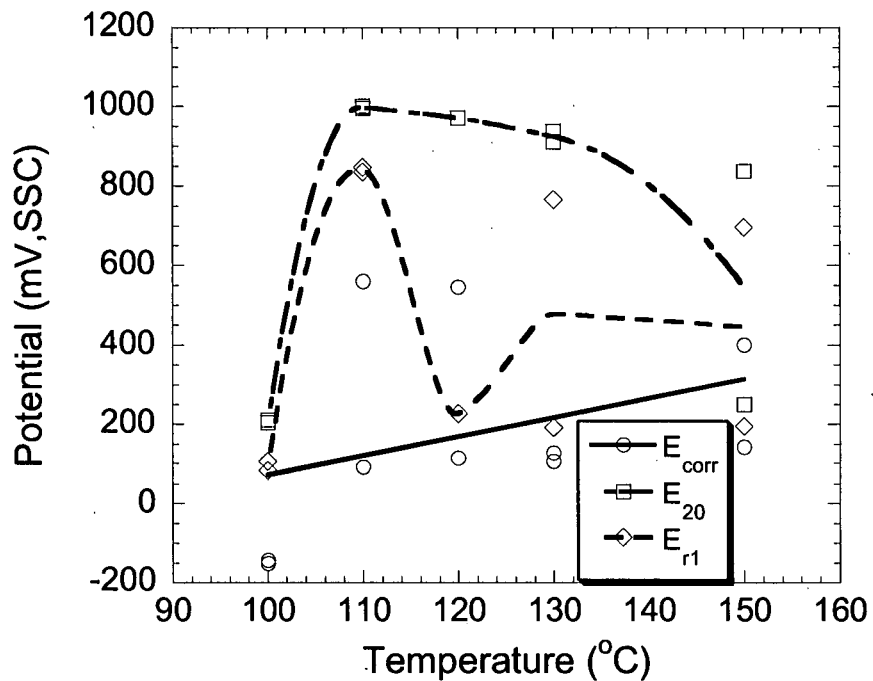


FIGURE 8 - E_{corr} , E_{20} and E_{r1} versus temperature for 12 molal CaCl_2 + 6 molal $\text{Ca}(\text{NO}_3)_2$.

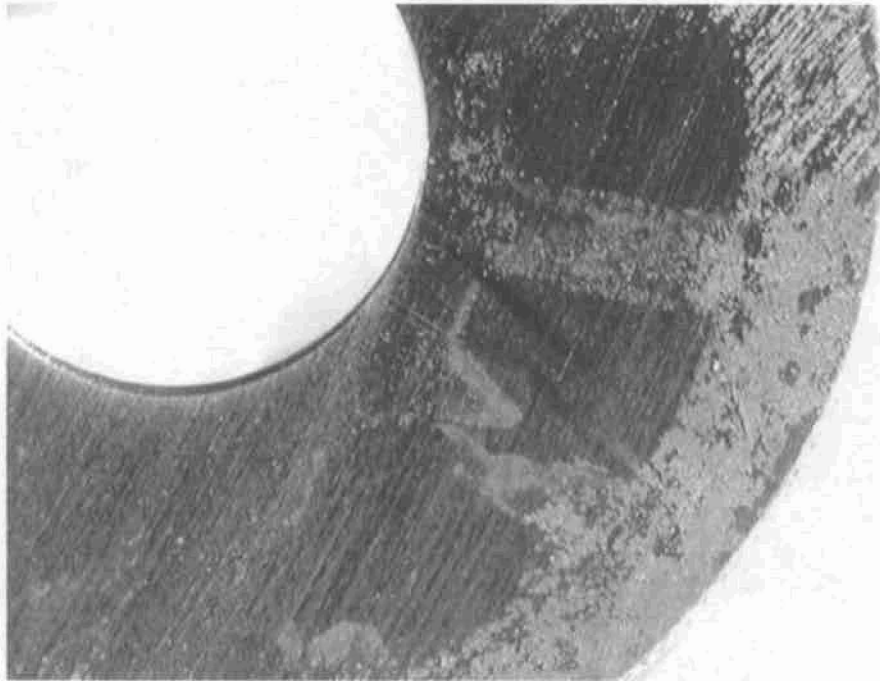


FIGURE 9 – Image of a specimen tested in 12 molal $\text{CaCl}_2 + 0.6$ molal $\text{Ca}(\text{NO}_3)_2$ at 130°C showing pitting outside of the crevice former region of the specimen. Lighter areas are pits. Outlining of crevice formers (trapezoidal shapes) is observed, but pitting does not show evidence of preferentially initiating at crevice formers. Magnification = 8X.

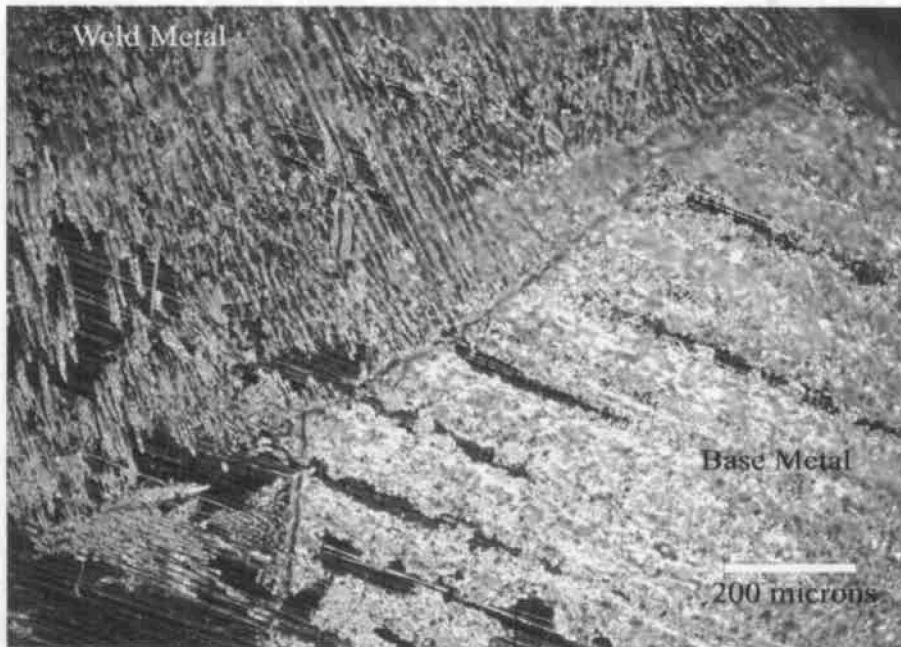


FIGURE 10 - Dark field image of specimen CP tested in 10 m $\text{CaCl}_2 + 1.5$ m $\text{Ca}(\text{NO}_3)_2$ at 100°C . The upper left of the image corresponds to weld metal and the lower right to base metal. Gray and light gray areas are pits. Magnification = 100X.